International Journal of Heat and Mass Transfer 81 (2015) 797–803

Contents lists available at ScienceDirect

International Journal of Heat and Mass Transfer

journal homepage: www.elsevier.com/locate/ijhmt

Modeling analysis on the silica glass synthesis in a hydrogen diffusion flame

Wei Yao [a], Lili Zheng [b], Hui Zhang [c,*]

[a] LHD, Institute of Mechanics, Chinese Academy of Sciences, Beijing 100190, PR China
[b] School of Aerospace, Tsinghua University, Beijing 100084, PR China
[c] Department of Engineering Physics, Tsinghua University, Beijing 100084, PR China

ARTICLE INFO

Article history:
Received 13 August 2013
Received in revised form 18 April 2014
Accepted 2 November 2014
Available online 20 November 2014

Keywords:
Silica glass
Flame hydrolysis deposition
Multiphase model
Modeling
Hydrogen flame

ABSTRACT

Silica glass ingot synthesis by flame hydrolysis deposition (FHD) is an important approach to obtain high-purity synthetic silica glass with high refractive index homogeneity. Using the precursor of silicon tetrachloride ($SiCl_4$), the silica ingot (SiO_2) can be synthesized in the oxy-hydrogen diffusion flame through a set of kinetic reactions and subsequent cooling. The homogeneity of the synthetic silica glass is influenced by the temperature/diameter equality of silica droplets and the residue of radicals (e.g. OH) in the synthetic silica. In this study, the mixing system of oxy-hydrogen diffusion flame and silica droplets in a furnace were modeled by a Euler–Lagrange multi-phase model, where the interphase exchange of mass, momentum and energy between the gas phase molecules and liquid phase silica droplets during the formation and transportation of silica droplets were included. The silica droplets were tracked by a Lagrangian formulation that includes the discrete phase inertia, hydrodynamic drag, the force of gravity and the dispersion due to turbulent eddies. The molecular gas phase reactions are described by a simple kinetic mechanism involving the major species during the formation of molecular SiO_2, with kinetic and thermodynamic parameters taken from the literature when available.

The effect of initial equivalence ratio on the flame structure was analyzed in the study, where the high-temperature region is uniform over the glass ingot and the OH residue is limited at unity equivalence ratio. The probability distributions of silica droplet diameter and temperature were analyzed by employing a developed droplet growth model, where the condensation rate is controlled by the in situ SiO_2 vapor concentration and the local flow-condition-determined mass transfer rate. The maximum diameter of silica droplets in the furnace is 1.39×10^{-4} m, and the percentage of silica droplets decreases with the increasing of diameter. Two high probability regions were observed for the droplet temperature distribution, the temperature below 1500 K accounts for 40% of the total droplet number, and the temperature range between 3500 and 4500 K accounts for 58%. The droplet diameter on the ingot cap distributes in the range from 4×10^{-5} to 9×10^{-5} m with approximately probability of 85%. The distribution of droplet temperature on the ingot cap is much uniform, with more than half (67%) of the droplets has the temperature between 3100 and 3200 K.

1. Introduction

Flame hydrolysis deposition (FHD) using silicon tetrachloride ($SiCl_4$) and oxy-hydrogen flame is an important approach to obtain high-purity synthetic silica glass with high refractive index homogeneity [1,2], which is crucially affected by the size, morphology and chemical composition of the formed silica droplets [3]. FHD method followed by a rapid consolidation at 1380 °C in vacuum ambiance has been shown to be capable of fabricating thick silica glass film up to 37 μm with a high deposition rate of 8 μm/min, which has a rather uniform refractive index 1.4456 ± 0.0005 in the wavelength 1500–1600 nm and a small absorption coefficient less than the magnitude of 10^{-7} in the wavelength 1300–1600 nm [4]. FHD, also called flame aerosol synthesis is a process involving combustion and aerosol science and engineering. Detailed diagnostic analysis of the process with the concurrent chemistry, transport and particle dynamics would inevitably advance the understanding and technical control of the manufacture of fumed silica. However, experimental diagnosis on the droplet existing multiphase flame is mainly limited by the short residence times of chemical reaction and particle growth, as well as the high process temperature [3]. Since the formation and growth of silica droplets are highly coupled with the temperature and species distribution in the flame, interaction between the gas

* Corresponding author. Tel.: +86 10 6279 2861; fax: +86 10 6279 2683.
E-mail address: zhhui@tsinghua.edu.cn (H. Zhang).

http://dx.doi.org/10.1016/j.ijheatmasstransfer.2014.11.004
0017-9310/

phase and the dispersed droplet phase should be included in the modeling to systematically investigate the effect of flame configuration on silica homogeneity.

The interacting effects of flame structure and silica formation have been experimentally and numerically investigated in the literature with different focuses. The thermophoretic transport of silica in chemical vapor deposition (CVD) processes was modeled but neglecting the counteraction of silica particles to the flame structure, where the uniformity and magnitude of the deposition are shown to be sensitive to the distance between the burner and the deposition target [5]. Temperature measurements in a silica-laden vapor axial deposition (VAD) flame by spontaneous Raman spectroscopy showed that the addition of silicon tetrachloride ($SiCl_4$) produces substantial changes in flame structure, i.e. rise of the thermal front [6]. Another spatially resolved temperature and OH radical concentration measurements in coflow oxy-hydrogen diffusion flames by coherent anti-Strokes Raman spectroscopy (CARS) and planar laser-induced fluorescence (PLIF) show that in the non-reacting zone temperature decreases due to the addition of $SiCl_4$, whereas in the silica formation zone flame temperature increases due to the exothermal hydrolysis and oxidation of $SiCl_4$ while the OH concentration decreases dramatically due to the reaction with HCl and the equilibrium shifts caused by the consumption of O_2 and H_2O in $SiCl_4$ related reactions [7]. The effect of silica formation on flame temperature and OH concentration was also experimentally and numerically observed in counterflow oxy-hydrogen flames [8], where the modeling incorporated detailed mechanism with H_2/O_2 reactions, silica generating reactions and chlorinated species reactions. Based on a modified kinetics mechanism for the combustion of $SiCl_4$ in an $H_2/O_2/Ar$ flame, the effect of $SiCl_4$ addition on the flame temperature and OH concentration was modeled and compared with the measurements by Laser-induced fluorescence (LIF) [9], where the underprediction of OH concentration is expected to be improved by considering particle formation and surface chemistry in the future study. Equilibrium analysis [9] also suggested that the flame temperature rise at $SiCl_4$ addition is mainly attributed to the condensation of silicon oxides since the heat release in the combustion of $SiCl_4$ is much small compared to that in the reaction between H_2 and O_2. A simple kinetic mechanism describing the formation of silica starting from the $SiCl_4$ combustion in high-temperature oxy-hydrogen flames were developed to reveal the impact of reaction channels on the overall reaction, where the reactivity of $SiCl_4$ towards H_2O is highly favored over its dissociation [10]. The deposition rate of synthetic silica glass in CVD processes is influenced by the available O_2 or H_2O amounts for oxidation or hydrolysis to completely covert $SiCl_4$ to spherical silica particles, however, whose size and microscopic morphology are observed independent of the carrier gas [11].

To improve the purity of synthetic silica glass, the turbulent combustion field in the furnace was modeled with the silica droplets involved. The effect of equivalence ratio on the turbulent flame structure was examined by employing a detailed mechanism of H_2–O_2 oxidation and $SiCl_4$ hydrolysis. The growth and transportation of silica droplets in the oxy-hydrogen diffusion flames in the furnace were modeled by considering the mass, momentum and energy exchanges between the gas and dispersed phases. The modeling results were analyzed to numerically suggest more preferable furnace configurations for silica synthesis.

2. Numerical model

2.1. Turbulent oxy-hydrogen flame modeling

The turbulent non-premixed oxy-hydrogen flame were modeled by Large Eddy Simulation (LES), where large eddies are resolved directly and small eddies are modeled. The Favre mean equations solved for mass, momentum, species and total enthalpy are given as,

$$\frac{\partial \bar{\rho}}{\partial t}+\frac{\partial}{\partial x_j}(\bar{\rho}\tilde{u}_j)=0 \tag{1}$$

$$\frac{\partial \bar{\rho}\tilde{u}_i}{\partial t}+\frac{\partial}{\partial x_j}(\bar{\rho}\tilde{u}_j\tilde{u}_i)=-\frac{\partial \bar{p}}{\partial x_i}+\frac{\partial}{\partial x_j}\left(\mu_{eff}\left(\frac{\partial \tilde{u}_i}{\partial x_j}+\frac{\partial \tilde{u}_j}{\partial x_i}-\frac{2}{3}\frac{\partial \tilde{u}_k}{\partial x_k}\delta_{ij}\right)\right)+\bar{\rho}g_i \tag{2}$$

$$\frac{\partial \bar{\rho}\widetilde{Y}_\alpha}{\partial t}+\frac{\partial}{\partial x_j}(\bar{\rho}\tilde{u}_j\widetilde{Y}_\alpha)=\frac{\partial}{\partial x_j}\left(\left(\bar{\rho}D_\alpha+\frac{\mu_t}{\sigma_t}\right)\frac{\partial \widetilde{Y}_\alpha}{\partial x_j}\right)+\bar{\omega}_\alpha \tag{3}$$

$$\frac{\partial \bar{\rho}\widetilde{H}}{\partial t}+\frac{\partial}{\partial x_j}(\bar{\rho}\tilde{u}_j\widetilde{H})=\frac{\partial}{\partial x_j}\left(\frac{\mu_t}{Pr_t}\frac{\partial \widetilde{H}}{\partial x_j}+\sum_\alpha h_\alpha\left(\rho D+\frac{\mu_t}{\sigma_t}\right)\frac{\partial \widetilde{Y}_\alpha}{\partial x_j}\right)+\bar{\omega}_H \tag{4}$$

where Boussinesq hypothesis has been employed here to parameterize the deviatoric part of the subgrid scale stress and the isotropic part was neglected assuming low Mac number. The turbulent Schmidt number and Prandtl number are both set as 0.85. The turbulent viscosity μ_t is given by Smagorinsky–Lilly model,

$$\mu_t=\bar{\rho}\cdot\min(\kappa d, C_s\Delta)^2\sqrt{2\widetilde{S}_{ij}\widetilde{S}_{ij}} \tag{5}$$

where the minimum function determines the mixing length for subgrid scales, κ is von Karman number constant, d is the distance to the closest wall, C_s is the Smagorinsky constant, Δ is the local grid scale, and $\widetilde{S}_{ij}$ is the viscous strain-rate tensor.

The mean production rate $\bar{\omega}_\alpha$ of species α by chemical reaction is calculated by the eddy-dissipation-concept (EDC) model [12] that incorporates detailed chemical mechanism for oxy-hydrogen and silica generating reactions in the turbulent flow. EDC assumes the reactions occur in fine turbulent scales with length fraction l^* and fine time scale τ^* (* denotes fine-scale quantities),

$$l^*=C_l\left(\frac{\nu\varepsilon}{\kappa^2}\right)^{1.4} \tag{6}$$

$$\tau^*=C_\tau\left(\frac{\nu}{\varepsilon}\right)^{1/2} \tag{7}$$

where constants $C_\xi=2.1377$, $C_\tau=0.4082$, ν – kinetic viscosity, κ – kinetic energy and ε – energy dissipation rate. Treating the fine scale as a constant pressure reactor, reactions proceed over the fine time scale τ^* with the initial condition of current species and temperature in the cell, reaching the final state with species mass fraction Y^*_α. The fine-scale reactions are governed by the Arrhenius rates. The mean production rate for species α is then calculated as,

$$\bar{\omega}_\alpha=\frac{\bar{\rho}l^{*2}}{\tau^*(1-l^{*3})}(Y^*_\alpha-Y_\alpha) \tag{8}$$

where l^{*3} represents the volume fraction of the fine scale. Detailed twenty-step oxy-hydrogen reaction mechanism from CHEMKIN model [13] plus reduced four-step $SiCl_4$ hydrolysis mechanism [10] is included in the volumetric reaction model, as listed in Table 1. The 15 involved species are H_2, H, O_2, O, OH, HO_2, H_2O_2, H_2O, $SiCl_4$, $SiCl_3OH$, $SiCl_2O$, SiClOOH, SiO_2, HCl and N_2.

The radiative heat transfer, mainly contributed by gas-phase H_2O, is solved by a Discrete Ordinate (DO) model [14], which solves the radiative transfer equation (RTE) for a finite number of discrete solid angles in the global Cartesian system. Each octant of the angular space is sectioned into two uniform extents in the polar and azimuthal angles respectively, and thus RTE in a total of $8\times2\times2$ directions are solved in the whole angular space 4π. Each control angle is further divided into 2×2 pixels to trace the energy incoming or outgoing to the face. Gray gas model is used in the modeling by assuming the scattering coefficient, the scattering phase function, and the refractive index are all independent of wavelength. The absorption coefficient as a function of species concentration, pressure and temperature is calculated by the weighted

Table 1
Rate constants used to model chemical reactions (units in J, kmol, s, m).

Reaction	$K = AT^n\exp(-E/RT)$		
	A	n	E
H_2/O_2 reactions			
$H_2 + O_2 = 2OH$	1.70E+10	0	2.00E+08
$OH + H_2 = H_2O + H$	1.17E+06	1.3	1.52E+07
$O + OH = O_2 + H$	4.00E+11	−0.5	0.00E+00
$O + H_2 = OH + H$	5.06E+01	2.67	2.63E+07
$H + O_2 + M = HO_2 + M$	3.61E+14	−0.72	0.00E+00
$H_2O/18.6/H_2/2.86/N_2/1.26/$			
$OH + HO_2 = H_2O + O_2$	7.50E+09	0	0.00E+00
$H + HO_2 = 2OH$	1.40E+11	0	4.49E+06
$O + HO_2 = O_2 + OH$	1.40E+10	0	4.49E+06
$2OH = O + H_2O$	6.00E+05	1.3	0.00E+00
$H + H + M = H_2 + M$	1.00E+15	−1	0.00E+00
$H_2O/0.0/H_2/0.0/$			
$H + H + H_2 = H_2 + H_2$	9.20E+10	−0.6	0.00E+00
$H + H + H_2O = H_2 + H_2O$	6.00E+13	−1.25	0.00E+00
$H + OH + M = H_2O + M$	1.60E+19	−2	0.00E+00
$H_2O/5/$			
$H + O + M = OH + M$	6.20E+13	−0.6	0.00E+00
$H_2O/5/$			
$O + O = O_2$	1.89E+10	0	−7.48E+06
$H + HO_2 = H_2 + O_2$	1.25E+10	0	0.00E+00
$HO2 + HO2 = H_2O2 + O2$	2.00E+09	0	0.00E+00
$H2O2 = OH + OH$	1.30E+17	0	1.90E+08
$H2O2 + H = HO2 + H2$	1.60E+09	0	1.59E+07
$H2O2 + OH = H2O + HO2$	1.00E+10	0	7.53E+06
Silica generating reactions			
$SiCl_4 + H_2O = SiCl_3OH + HCl$	8.20E+11	0	1.28E+08
$SiCl_3OH = SiCl_2O + HCl$	2.80E+13	0	2.09E+08
$SiCl_2O + H_2O = SiClOOH + HCl$	2.40E+12	0	7.00E+07
$SiClOOH = SiO_2 + HCl$	3.70E+13	0	2.05E+08

sum of gray gases model (WSGGM) [15], which improves the accuracy of gray gas model through weighted sum the mean absorption coefficient over continuous gray gas bands.

2.2. Discrete model and gas–liquid interaction

The liquid silica droplets formed and dispersed in the furnace are modeled by the Euler–Lagrange discrete model, where the gas phase is treated as a continuum by solving the Navier–Stokes equations, while the dispersed phase is solved by tracking a large number of droplets through the calculated flow field. As a gas–liquid interaction, the dispersed phase can exchange momentum, mass, and energy with the gas phase. The trajectory of liquid droplets is tracked by integrating the force balance in the Lagrangian framework. The force balance equation acting on the droplets is written as,

$$\frac{d\vec{U}_d}{dt} = F_D(\vec{U} - \vec{U}_d) + \frac{\vec{g}(\rho_d - \rho)}{\rho_d} + \vec{F}_T + \vec{F}_B + \vec{F}_S \quad (9)$$

where $\vec{U}$ and $\vec{U}_d$ are gas phase and droplet velocities, the first and second terms in the right hand side represent the drag force per unit droplet mass and the gravity force, $\vec{F}_T$ – the thermophoretic force due to temperature gradient, $\vec{F}_B$ – the Brownian force for submicron droplets and $\vec{F}_S$ – the Saffman's lift force due to shear.

A droplet growth model was developed to model the conversion of gas phase silica into liquid silica droplets. The mass flux condensed from the gas phase to the droplet surface is governed by gradient diffusion,

$$\dot{m}_{silica} = (2 + 0.6Re^{1/2}Sc^{1/3})\Gamma/D(C_\infty - C_s) \quad (10)$$

where C_∞ is the SiO_2 concentration in the bulk gas, C_s is assumed to be zero as the vapor concentration of silica at the droplet surface. The mass transfer coefficient before the concentration terms in the parentheses is given by the Sherwood number correlation [16,17] with Re the Reynolds number, Sc the Schmidt number, D the droplet diameter and Γ the diffusion coefficient of SiO_2 in the bulk gas. The mass flux given by Eq. (10) becomes the source in the gas phase species transport equation of SiO_2, and the mass of droplet increases accordingly.

During the transport and growth, the droplet temperature is assumed uniform temperature throughout and simply determined by the heat balance related to the convective heat transfer, the radiative absorption/emission at the particle surface and the latent heat of condensation when SiO_2 vapor condenses to form liquid silica droplets.

Since the mass and momentum loading in the silica droplets become significant as the silica droplets grow, a two-phase coupling is followed to include the important impact of the discrete phase on the continuous phase flow field. During the trajectory simulation, the heat, mass, and momentum gained or lost by the particle stream are tracked and incorporated into the subsequent continuous phase calculations. The mass, heat and momentum transfers from the continuous phase to the discrete phase is calculated by examining the changes in mass, momentum and internal energy of a droplet as it passes through each control volume. These interphase exchange terms are integrated for all passing droplets in each control volume, and then impact the continuous phase by acting as source terms of corresponding governing equations. An iteration procedure is used in solving the discrete and continuous phase equations until the solutions in both phases are unchanged in each physical time step. In this study, unsteady droplet tracking is conducted with the same time step of continuous flow calculation, and the discrete phase iteration is performed once every time step.

To simulate the nucleation process in silica droplet formation, a large number of micro seeds need to be provided in advance to sustain the subsequent mass growth. The requirements for setting initial seeds are: (1) small in both mass and volume to less impact the continuous phase, (2) but large in number density to ensure at least one seed is provided for each reacting volume cell. In this study, a micro size of 1×10^{-6} m is selected for initial seeds, since the sizes of most silica droplets observed in industrial process are above the order of magnitude of 1×10^{-5} m. The total flow rate of initial silica seeds is 1×10^{-11} kg/s, thus the release seed rate is 8685 per second assuming a constant density of 2200 kg/s for liquid silica. The seeds are injected normal to the injector surface with a small velocity of 0.1 m/s, and then gain higher velocity through momentum exchange with the continuous gas flow stream.

3. Results and discussion

3.1. Effect of initial equivalence ratio

Fig. 1 shows the geometry configuration of the injector pan, which has a diameter of 0.08 m. Eight and sixteen 3-mm-diameter oxygen orifices are evenly aligned on the first and the second O_2 rings. The two oxygen rings have diameters of 0.03 and 0.05 m respectively, and both center at a 3.6-mm-diameter center orifice, from which $SiCl_4$ and O_2 mixture is injected. In addition, oxygen curtains are injected from the outer ring with a width of 2 mm and the inner ring with a width of 1.2 mm. The injection rate of $SiCl_4$ is 4.2×10^{-4} kg/s from the center orifice. The oxygen streams are injected uniformly at a total rate of 5.3×10^{-3} kg/s from the center orifice, and the inner, first, second and outer rings, while pure hydrogen fuel is injected uniformly from the remaining area of the injector pan.

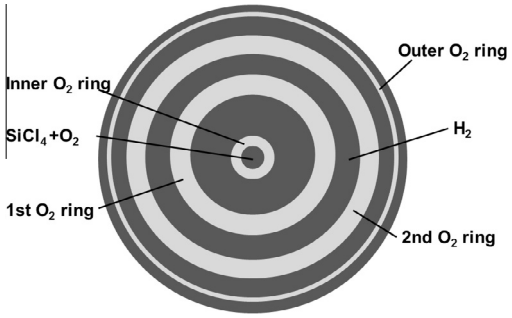

Fig. 1. The geometry configuration of the injector.

Fig. 2 shows the temperature field on the centerplane of the furnace corresponding to different equivalence ratios, i.e. 0.5, 1.0 and 2.0. From the figure, the shown high-temperature region 2900–4500 K in the turbulent jet flame is obviously thinner under fuel-lean condition, while the overall temperature in the shown high-temperature region is quite lower for the equivalence ratio case of 2.0 than for the case of stoichiometric ratio. Apart from the shown high-temperature (2900–4500 K) flame region, the mean temperature in the other regions of the furnace is above 2000 K. In this study, the equivalence ratio is increased by increasing the fuel flow rate while maintaining the same oxygen flow rate, thus the high-temperature gases span more around the ingot cap with the increasing of equivalence ratio. From Fig. 2, the temperature is generally higher at the base of oxygen jet streams, where the hydrogen initially mixes with oxygen to react. The temperature is the highest in the center oxygen jet stream, where the exothermic reactions between $SiCl_4$ and H_2O further promote the temperature rise. Under both fuel lean and rich conditions, the temperature reaching the glass ingot is lower than the case with unity equivalence ratio. Table 2 shows that the peak temperature is the highest under the condition of unity equivalence ratio, while the peak temperature is 300 K lower under fuel lean condition and 200 K lower under fuel rich condition. Note that the reduced four-step $SiCl_4$ hydrolysis mechanism [10] somewhat overestimated the peak temperatures compared with the values experienced in industrial furnace, therefore more detailed mechanisms needs to be developed to accurately reproduce the temperature field in the future study. A broader yet uniform high-temperature region is of benefit for the synthesis of high purity silica since the temperature gradient is smaller in the top part of furnace, which is the main silica-formation region. As described above, the high temperature region becomes broader with increasing of equivalence ratio, but the temperature gradient from the center oxygen stream to the outer region increases at the equivalence ratio of 2.0. The slight

Table 2
The maximums of temperature, SiO_2, HCl and OH mass fractions in the furnace for different initial equivalence ratios.

Equivalence ratio	T_{max} (K)	SiO_2	HCl	OH
0.5	4692	0.1829	0.443	3.47e−8
1	4989	0.1926	0.466	2.97e−8
2	4794	0.1917	0.464	2.67e−8

asymmetry of temperature fields shown in Fig. 2 is caused by that the centerplane through the two lateral outlet vents did not exactly cut the injector pan into two symmetric parts. The location of orifices on the first and second oxygen rings was not deliberately designed to align with the centerplane, since the injector pan in real industrial process is a movable part and the influence on the flame uniformity is generally negligible as long as more orifices are designed or the injector pan is rotated, whose effects will be investigated in the future study.

Intermediate radicals and species, such as OH and SiO_2, were predicted by the detailed mechanism of hydrogen oxidation and $SiCl_4$ hydrolysis. SiO_2 is mainly produced in the center oxygen jet stream carrying $SiCl_4$, and Table 2 shows that both deficient and excess hydrogen tends to inhibit its production and the peak concentration is the highest at the unity equivalence ratio. Under fuel lean condition, the concentration of H_2O reduces, and correspondingly the production of SiO_2 decreases. Under fuel rich condition, the lower flame temperature inhibits the production of SiO_2. The HCl concentration characterizes conversion of $SiCl_4$ towards SiO_2. Restricted by the lower H_2O concentration under fuel lean condition, the HCl concentration is clearly reduced. Under fuel rich condition, the H_2O concentration is roughly the same as the unity equivalence ratio case, but the lower temperature of reacting stream prohibits the conversion of $SiCl_4$ with H_2O towards SiO_2. OH is minimum under the condition of stoichiometric ratio. The OH concentration has its peak value at the base of oxygen streams, and decreases gradually downstream. The peak OH concentration decreases with the increasing of equivalence ratio, due to the consumption of OH by excess H_2. The OH concentration predicted on the glass ingot is in the order of magnitude of 1×10^{-9}, which is in accordance with the small hydroxyl concentration in the synthetic silica [18].

In sum, the high-temperature region is generally broad enough to cover the ingot cap while a small temperature gradient can be maintained in the ensemble reacting stream for the unity equivalence ratio; the residue of OH at unity equivalence ratio is between those under fuel lean and fuel rich conditions. From the comparison, the combustion field at a unity equivalence ratio is more preferable for silica synthesis due to its homogeneous temperature field over the ingot cap and limited OH residue.

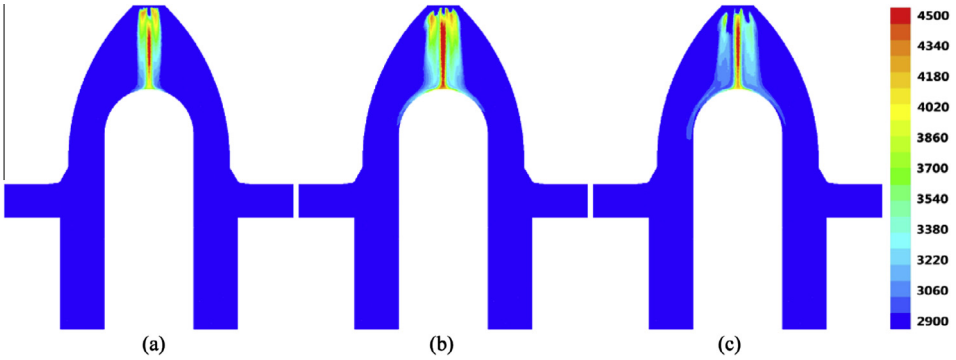

Fig. 2. Temperature field (K) on the centerplane for the equivalence ratio of (a) 0.5, (b) 1.0 and (c) 2.0.

3.2. Liquid droplet growth

Fig. 3(a) shows the distribution of silica droplet with different sizes in the combustion field of the furnace at the initial equivalence ratio of unity. The silica droplets grow from micro seeds with the diameter of 1×10^{-6} m released from the orifices along with the fuel and oxygen streams. The movements of droplets along their trajectories are affected by the balance of acting forces, which includes drag force, gravity force, thermophoretic force, Brownian force and Saffman's lift force. As the droplets travel along their trajectories, the SiO_2 vapor in the gas phase gradually condenses on the silica droplets to increase the droplet diameter. The mass transfer rate from the bulk gas to the silica droplet is controlled by the local concentration of SiO_2 vapor, and the condensation process correspondingly reduces the SiO_2 concentration in the gas phase. The droplet trajectories are generally along with the reacting stream, and the droplets in the downstream have larger sizes due to growth. In the modeling, all the wall surfaces of furnace shell and glass ingot are assumed to be trap boundary, i.e. the droplets will adhere to the wall to terminate the trajectory calculations. Part of silica droplets will escape form the furnace outlets. In the transient calculation, the release of new droplet seeds and the trap/escape of droplets on the wall/outlet boundaries can reach a quasi-steady state. Fig. 3(b) shows the probability distribution of droplet diameters in the furnace when reaching the quasi-steady state. The maximum diameter of silica droplets is 1.39×10^{-4} m, and the mean diameter is 3.08×10^{-5} m. From the probability distribution, the small droplets with diameters less than 1.0×10^{-5} m take more than 80% of the total number. The percentage of larger droplets decreases with the increasing of diameter, since that only few droplets can travel long trajectories to grow before the cease when encountering a wall or outlet surface. The percentage of droplets with diameters larger than 5.0×10^{-5} m is less than 1%, which are mainly distributed below the ingot cap as shown in Fig. 3(a).

Fig. 4 shows the droplet distribution contoured by droplet temperature. The droplet temperature is determined by a heat balance relating to the convective heat transfer and the absorption/emission of radiation at the droplet surface. As can be seen, the droplets have the initial temperature of 300 K at the base of reacting stream, after that the droplet temperature increases to around 4000 K to balance with the flame temperature as the droplets travel in the high-temperature region. As the droplets travel further downstream with the reacting stream, the droplet temperature decreases due to convective and radiative cooling but is still above 3000 K. The mean droplet temperature is 2409 K. Fig. 4(b) shows the probability distribution of droplet temperature, where two high probability regions are observed. The first high probability region from 300 to 1500 K corresponds to those droplets at the base of the fuel/oxygen streams before the start of fierce combustion reaction. The droplet velocities at the stream base are generally low with only the initial cold stream velocity, therefore a large number of cold droplets are accumulated there to form the first high probability region accounting for 40% of the total number. As the droplets enter the high-temperature region, they quickly obtain the high temperature of reacting stream, and those high-temperature droplets do not get the opportunity to be cooled down sufficiently to below 1500 K before the termination of their trajectories. The second high probability region from 3000 to 4500 K takes around 58% of the total droplet number. Those droplets with temperature from 1500 to 2500 K account for 3%, and those with extremely high temperature above 4500 K account for only 0.1% of the total number. As suggested in [9] that the condensation of silicon oxides brings the total heat release up to about the same amount as for the water formation, while the heat release during the exothermic reactions of $SiCl_4$ hydrolysis can be ignored compared to that for the combustion of H_2 and O_2. The thermal effect of condensation was considered in the modeling by adding the latent heat of condensation as the source term of heat balance equation for growing droplets. The thermal effect of condensation is obvious since the maximum droplet temperature reaches 5000 K, which is higher than the peak flame temperature (4989.08 K) predicted without considering the silica droplet formation.

Fig. 5 shows the probability distributions of diameter and temperature for silica droplets on the ingot cap. The droplet diameter distributes in the range from 4×10^{-5} to 9×10^{-5} m with approximately probability of 85%. The percentage of droplets with diameter less than 4×10^{-5} m is 5% and that with diameter larger than 9×10^{-5} m is 10% in total. The maximum and minimum of droplet diameter are 1.37×10^{-4} and 2.83×10^{-5} m respectively, with the mean diameter of 6.61×10^{-5} m. The distribution of droplet temperature on the ingot cap is much uniform, with most (67%) of the droplets has the temperature between 3100 and 3200 K. The droplets in the temperature ranges below 3100 K, and between 3200 and 3400 K, are both 12% in the number percentage. The droplets with temperature above 3400 K account for 9% in total. The maximum and minimum of droplet temperature are 4309 and 3023 K respectively, with the mean droplet temperature of 3225 K on the ingot cap.

The homogeneity of droplet temperature on the ingot cap is generally satisfactory, but the diameter equality needs to be improved in the current furnace design. Since the condensation rate is in a large part controlled by the SiO_2 vapor concentration,

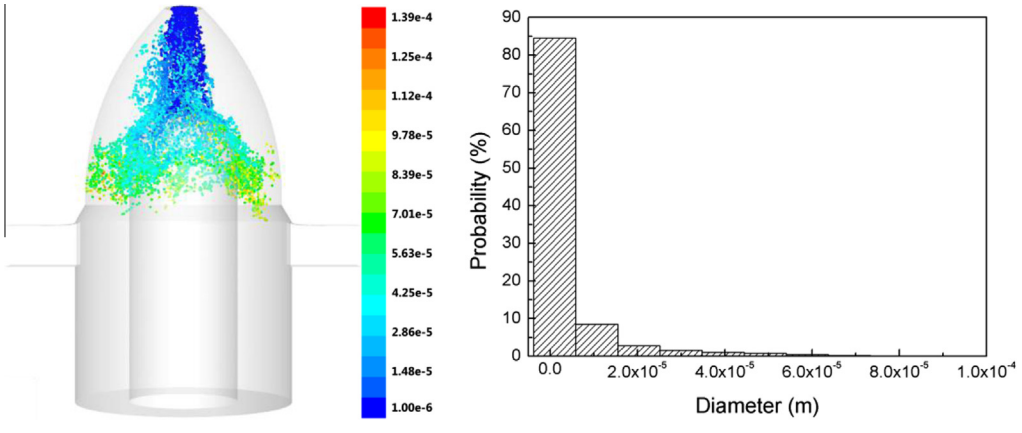

Fig. 3. (a) The distribution of silica droplets with different sizes (m) in the furnace, and (b) the probability distribution of silica droplet diameters.

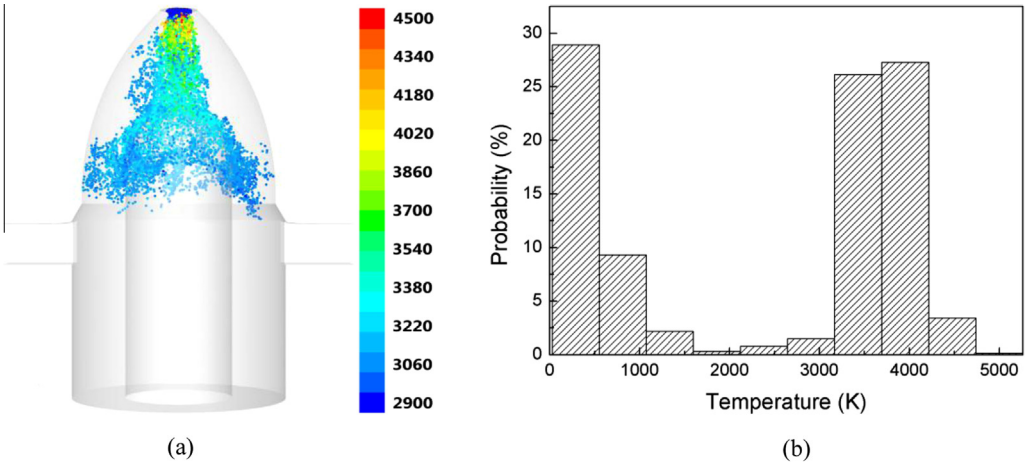

Fig. 4. (a) The distribution of silica droplets with different temperature (K) in the furnace, and (b) the probability distribution of silica droplet temperature.

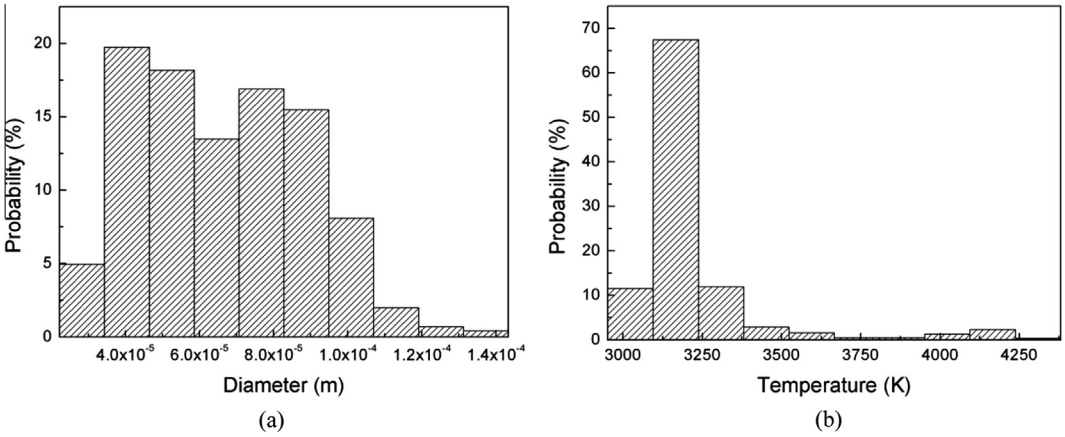

Fig. 5. The probability distributions of (a) droplet diameter and (b) droplet temperature on the ingot cap.

the carrier gas stream of $SiCl_4$ should be configured in the burner to span the SiO_2 vapor more uniformly in the reacting stream. As noticed in Fig. 3(a), large droplets with diameter higher than 7×10^{-5} m are mainly distributed around the ingot column but below the ingot cap, to avoid the adherence of those large droplets on the ingot column, a trap or exhaust apparatus can be installed surrounding to the main reacting stream and the ingot column to filter those large droplets. To further uniform the droplet temperature, on effective is to reduce the temperature gradient in the reacting stream. A further splitting of the oxygen streams through more orifices is one possible solution in unifying the temperature in the reacting stream. By aid of the multi-phase droplet growth model developed in this study, more influencing aspects of flame structure on the diameter and temperature distributions of silica droplets can be analyzed in the future study to further optimize the FHD process in the industrial furnace.

4. Conclusion

In this study, the Euler–Lagrange multi-phase model has been applied to model the formation and transport of silica droplets in a coflow oxy-hydrogen diffusion flame with $SiCl_4$ addition by incorporating the interactions between flame structure and silica formation. The flame structure at different initial equivalence ratios was analyzed firstly to determine the suitable combustion field for the generation and deposition of silica droplets. The mass, momentum and energy exchange between the dispersed phase and the gas-phase was modeled to obtain a realistic silica droplet distribution in the furnace.

The width of high-temperature region increases with the increasing of equivalence ratio since the fuel flow rate increases, but the ensemble temperature in the high-temperature region decreases under fuel rich condition. The peak temperature at the unity equivalence ratio is 300 K higher than at the equivalence ratio of 1.0 (fuel lean condition) and 200 K higher than that at the equivalence ratio of 2.0 (fuel rich condition). The conversion of $SiCl_4$ towards SiO_2 through hydrolysis is the highest at unity equivalence ratio, but the OH concentration is effectively suppressed by the excess H_2 under fuel rich condition. To accurately reproduce the flame temperature field, more detailed $SiCl_4$ hydrolysis mechanisms need to be developed for the gas phase prediction in the future study.

The probability distributions of droplet diameter and temperature in the whole furnace and on the glass cap were analyzed when the generation and termination of silica droplets reaching a quasi-steady state. The maximum diameter of silica droplets in the furnace is 1.39×10^{-4} m, and the mean diameter is 3.08×10^{-5} m. The small droplets with diameters less than 1.0×10^{-5} m take more than 80% of the total number. The percentage of silica droplets decreases with the increasing of diameter. For the droplet temperature distribution, two high probability regions were observed, the temperature below 1500 K accounts for 40% of the total droplet number, and the temperature range between 3000

and 4500 K accounts for 58%. The thermal effect of condensation increases the maximum droplet temperature to 5000 K, which is higher than the peak flame temperature (4989.08 K) without considering the silica droplet formation. The droplet diameter on the ingot cap distributes in the range from 4×10^{-5} to 9×10^{-5} m with approximately probability of 85%. The distribution of droplet temperature on the ingot cap is much uniform, with more than half (67%) of the droplets has the temperature between 3100 and 3200 K, and 12% of the droplets respectively in the temperature ranges below 3100 K, and between 3200 and 3400 K.

A droplet growth model was developed in this study, where the condensation rate is controlled by the in situ SiO_2 vapor concentration and the local flow-condition-determined mass transfer rate. The movements of droplets along their trajectories are affected by the balance of acting forces, which includes drag force, gravity force, thermophoretic force, Brownian force and Saffman's lift force. The droplet temperature is determined by the convective and radiative heat exchange with the surrounding gas phase at the droplet surface, as well as the heat released during vapor condensation. In addition to the fuel/oxygen ratio, more configurations on the burner and the furnace will be examined using the developed multi-phase droplet growth model in order to optimize the FHD process for producing high-purity synthetic silica glass using $SiCl_4$ and oxy-hydrogen flame.

Conflict of interest

None declared.

Acknowledgment

This work was partially supported by National Basic Research Program of China (973 Program No: 2012CB719705).

References

[1] D. Lee, M. Choi, Control of size and morphology of nano particles using CO_2 laser during flame synthesis, J. Aerosol Sci. 30 (1999) S491–S492.
[2] D. Lee, M. Choi, Coalescence enhanced synthesis of nanoparticles to control size, morphology and crystalline phase at high concentrations, J. Aerosol Sci. 33 (2002) 1–16.
[3] S.E. Pratsinis, Flame aerosol synthesis of ceramic powders, Prog. Energy Combust. Sci. 24 (1998) 197–219.
[4] Y. Wu, H. Xing, L. Zhang, A. Li, W. Zheng, G. Liu, Y. Guo, Y. Zhang, Fabrication and properties of vitreous silica films prepared by flame hydrolysis deposition, Mater. Chem. Phys. 84 (2004) 234–237.
[5] H.C. Tsai, R. Greif, S. Joh, A study of thermophoretic transport in a reacting flow with application to external chemical vapor deposition processes, Int. J. Heat Mass Transfer 38 (1995) 1901–1910.
[6] M.D. Allendorf, J.R. Bautista, E. Potkay, Temperature measurements in a vapor axial deposition flame by spontaneous Raman spectroscopy, J. Appl. Phys. 66 (1989) 5046–5051.
[7] J.Y. Hwang, Y.S. Gil, J.I. Kim, M. CHoi, S.H. Chung, Measurements of temperature and OH radical distributions in a silica generating flame using CARS and PLIF, J. Aerosol Sci. 32 (2001) 601–613.
[8] J.I. Kim, J.Y. Hwang, J. Lee, M. Choi, S.H. Chung, Numerical and experimental study on silica generating counterflow diffusion flames, Int. J. Heat Mass Transfer 48 (2005) 75–81.
[9] T. Moore, B. Brady, L.R. Martin, Measurements and modeling of $SiCl_4$ combustion in a low-pressure H_2/O_2 flame, Combust. Flame 146 (2006) 407–418.
[10] B. Hannebauer, F. Menzel, The combustion of $SiCl_4$ in hot O_2/H_2 flames, Z. Anorg. Allg. Chem. 629 (2003) 1485–1490.
[11] C. Xu, Z.a. GU, C. Rao, Influence of carrier gas on the deposition rate of synthetic silica glass by chemical vapor deposition method, J. Chin. Ceram. Soc. 37 (2009) 1796–1802.
[12] B.F. Magnussen, On the structure of turbulence and a generalized Eddy dissipation concept for chemical reaction in turbulent flow, in: 19th American Institute of Aeronautics and Astronautics Aerospace Science Meeting, St. Louis, Missouri, 1981.
[13] R.J. Kee, F.M. Rupley, J.A. Miller, M.E. Coltrin, J.F. Grcar, E. Meeks, H.K. Moffat, A.E. Lutz, G. Dixon-Lewis, M.D. Smooke, J. Warnatz, G.H. Evans, R.S. Larson, R.E. Mitchell, L.R. Petzold, W.C. Reynolds, M. Caracotsios, W.E. Stewart, P. Glarborg, C. Wang, C.L. McLellan, O. Adigun, W.G. Houf, C.P. Chou, S.F. Miller, P. Ho, P.D. Young, D.J. Young, D.W. Hodgson, M.V. Petrova, K.V. Puduppakkam, CHEMKIN Release V4.1, in, Reaction Design Inc., San Diego, CA, 2006.
[14] E.H. Chui, G.D. Raithby, Computation of radiant heat transfer on a non-orthogonal mesh using the finite-volume method, Numer. Heat Transfer Part B: Fundam. 23 (1993) 269–288.
[15] T.F. Smith, Z.F. Shen, J.N. Friedman, Evaluation of coefficients for the weighted sum of gray gases model, J. Heat Transfer 104 (1982) 602–608.
[16] W.E. Ranz, J.W.R. Marshall, Evaporation from drops, Part I, Chem. Eng. Prog. 48 (1952) 141–146.
[17] W.E. Ranz, J.W.R. Marshall, Evaporation from drops, Part I and Part II, Chem. Eng. Prog. 48 (1952) 173–180.
[18] Y. Zhou, Study on hydroxyl in quartz glass and quartz raw materials, in, China Building Materials Academy, 2002.